JGR Atmospheres

RESEARCH ARTICLE
10.1029/2021JD034827

Special Section:
The Arctic: An AGU Joint Special Collection

Surface Heat and Moisture Exchange in the Marginal Ice Zone: Observations and a New Parameterization Scheme for Weather and Climate Models

A. D. Elvidge[1], I. A. Renfrew[1], I. M. Brooks[2], P. Srivastava[2,3], M. J. Yelland[4], and J. Prytherch[5]

[1]School of Environmental Sciences, University of East Anglia, Norwich, UK, [2]School of Earth and Environment, University of Leeds, Leeds, UK, [3]Centre of Excellence in Disaster Mitigation and Management, Indian Institute of Technology Roorkee, Roorkee, India, [4]National Oceanography Centre, Southampton, UK, [5]Department of Meteorology, Stockholm University, Stockholm, Sweden

Abstract Aircraft observations from two Arctic field campaigns are used to characterize and model surface heat and moisture exchange over the marginal ice zone (MIZ). We show that the surface roughness lengths for heat and moisture over uninterrupted sea ice vary with *roughness Reynolds number* (R_*; itself a function of the roughness length for momentum, z_0, and surface wind stress), with a peak at the transition between aerodynamically *smooth* (R_*<0.135) and aerodynamically *rough* (R_*>2.5) regimes. A pre-existing theoretical model based on surface-renewal theory accurately reproduces this peak, in contrast to the simple parameterizations currently employed in two state-of-the-art numerical weather prediction models, which are insensitive to R_*. We propose a new, simple parameterization for surface exchange over the MIZ that blends this theoretical model for sea ice with surface exchange over water as a function of sea ice concentration. In offline tests, this new scheme performs much better than the existing schemes for the *rough* conditions observed during the 'Iceland Greenland Seas Project' field campaign. The bias in total turbulent heat flux across the MIZ is reduced to only 13 W m^{-2} for the new scheme, from 48 and 80 W m^{-2} for the Met Office Unified Model and ECMWF Integrated Forecast System schemes, respectively. It also performs marginally better for the comparatively *smooth* conditions observed during the 'Aerosol-Cloud Coupling and Climate Interactions in the Arctic' field campaign. The new surface exchange scheme has the benefit of being physically-motivated, comparatively accurate and straightforward to implement, although to reap the full benefits an improvement to the representation of sea ice topography via z_0 is required.

Key Points:

- Observations over the marginal ice zone show that surface scalar exchange is a function of the aerodynamic roughness of the surface
- Existing scalar exchange parameterization schemes do not represent this sensitivity; we propose a new scheme that does
- The new scheme is more accurate in offline calculations of surface heat fluxes, especially for aerodynamically rough conditions

Correspondence to:
A. D. Elvidge,
a.elvidge@uea.ac.uk

Citation:
Elvidge, A. D., Renfrew, I. A., Brooks, I. M., Srivastava, P., Yelland, M. J., & Prytherch, J. (2021). Surface heat and moisture exchange in the marginal ice zone: Observations and a new parameterization scheme for weather and climate models. *Journal of Geophysical Research: Atmospheres*, *126*, e2021JD034827. https://doi.org/10.1029/2021JD034827

Received 4 MAR 2021
Accepted 2 AUG 2021

1. Introduction

In the polar regions, sea ice provides a topographic obstacle to airflow, resulting in the generation of turbulence in the atmospheric boundary layer (Notz, 2012). It is also associated with strong gradients in surface properties such as temperature and humidity where it borders water, in what is known as the Marginal Ice Zone (MIZ). The turbulence and strong vertical gradients result in elevated surface fluxes of momentum, heat and moisture, which exert a significant influence on the weather and climate of the mid- to high-latitudes (e.g., Rae et al., 2014; Renfrew, Elvidge, & Edwards, 2019; Pope et al., 2020); on ocean circulation and deep water formation (e.g., Renfrew et al., 2019, 2021; Stössel et al., 2008); and on the extent, thickness and transport of sea ice (e.g., Fichefet & Maqueda, 1997; Tsamados et al., 2014; Vavrus & Harrison, 2003). In numerical weather prediction (NWP), climate, and sea-ice models, these surface fluxes must be parameterized.

Momentum flux (or *drag*) over a rough surface can be partitioned into two components: a *skin* component due to surface friction, and a *form* component due to the pressure force exerted on the airflow by roughness elements (Arya, 1973, 1975). Over sea ice, roughness elements include the vertical edges of ice floes and melt ponds, pressure ridges, and other topographic features resulting from sea-ice dynamics. In the MIZ, peak values typically occur at ice fractions of 0.5–0.8, where the surface is roughest owing largely to the ice floe edges (Andreas, Horst, et al., 2010; Elvidge et al., 2016; Held et al., 2011; Lüpkes & Birnbaum, 2005). A series of physically based parameterization schemes have been developed over several decades that provide the neutral drag coefficient, C_{DN}, as the sum of three components: drag from ice-free water (C_{DNw}), drag from uninterrupted sea ice (C_{DNi}), and the form drag against ice floe edges across the MIZ (C_{DNf}; Arya, 1973, 1975;

Birnbaum & Lüpkes, 2002; Garbrecht et al., 2002; Lüpkes & Gryanik, 2015; Lüpkes et al., 2012). These can be combined for ice fraction, A, as follows:

$$C_{\mathrm{DN}} = \left(1 - A\right)C_{\mathrm{DNw}} + A\,C_{\mathrm{DNi}} + C_{\mathrm{DNf}}. \tag{1}$$

Schemes using this framework have been validated and modified using aircraft and tower observations (e.g., Elvidge et al., 2016; Lüpkes & Birnbaum, 2005) and have recently been implemented in a range of numerical models, including the Met Office Unified Model (MetUM; Renfrew, Elvidge, & Edwards, 2019), the European Centre for Medium-Range Weather Forecasts Integrated Forecast System (IFS; Roberts et al., 2018), the Los Alamos Sea Ice Model (CICE; Tsamados et al., 2014), and a regional coupled climate model (HIRHAM–NAOSIM 2.0; Yu et al., 2020). In the parameterization schemes of NWP models such as the MetUM and IFS, C_{DNf} is typically provided simply as a function of ice fraction, C_{DNi} is fixed, and C_{DNw} is provided by a separate air-sea exchange scheme that is a function of wind speed. Elvidge et al. (2016) demonstrated that this configuration is capable of accurately representing drag across the marginal ice zone, but that variability in C_{DNi} remains a major source of uncertainty which is currently unaccounted for in parameterization schemes. The large variability in C_{DNi} (i.e., sea ice topography) has also been highlighted in other observational studies (e.g., Castellani et al., 2014; Petty et al., 2017).

The theoretical framework for scalar (heat and moisture) exchange over the MIZ has received less attention than that for momentum exchange. On the basis of a surface-renewal model, Andreas (1987; hereafter A87) derived a theoretical conceptual model for scalar exchange over ice and snow surfaces for both aerodynamically *rough* and *smooth* regimes. Here, aerodynamic roughness is defined by the *roughness Reynolds number*—the ratio of characteristic roughness height to the viscous length-scale of the flow:

$$R_* = \frac{z_0 u_*}{\nu}, \tag{2}$$

where z_0 is the surface roughness length for momentum, u_* is the friction velocity (which is positively correlated with windspeed), and ν is the kinematic viscosity of the surface layer flow. z_0 is related to C_{DN} as follows:

$$C_{\mathrm{DN}} = \frac{\kappa^2}{\ln\left(z/z_0\right)^2}, \tag{3}$$

where κ is the von Karman constant (0.4) and z is the reference height at which the exchange coefficient is evaluated (typically 10 m). In a *rough* regime ($R_* \geq 2.5$; relatively strong winds over a rough surface), turbulent eddies sweep into the interfacial sublayer, causing air to become trapped between roughness elements for a short period of time. In a *smooth* regime ($R_* \leq 0.135$; relatively weak winds over a smooth surface), impinging eddies remain in motion. Accordingly, A87 employs a molecular diffusion model to represent scalar exchange in the *rough* regime; whilst an advective diffusion model is employed in the *smooth* regime. A87 also identifies a third, *transitional* regime. The A87 model provides the ratios of each of the scalar roughness lengths to the momentum roughness length (z_{0T}/z_0 for heat; z_{0q}/z_0 for moisture) as functions of R_* (see Figure 8 in A87). The scalar exchange coefficients (C_{HN} for heat and C_{EN} for moisture) and consequently the sensible and latent heat fluxes (SH and LH, respectively) are then provided by Monin Obukhov similarity theory as:

$$C_{\mathrm{HN}} = \frac{\kappa^2}{\ln\left(z/z_0\right)\ln\left(z/z_{0T}\right)}, \tag{4}$$

$$C_{\mathrm{EN}} = \frac{\kappa^2}{\ln\left(z/z_0\right)\ln\left(z/z_{0q}\right)}, \tag{5}$$

$$\mathrm{SH} = c_p\,\rho\,C_{\mathrm{HN}}\,U\left(\theta_s - \theta\right), \tag{6}$$

$$\mathrm{LH} = L_V \rho C_{\mathrm{EN}} U \left(q_s - q\right), \tag{7}$$

where ρ is air density; U is wind speed; $\theta_s - \theta$ and $q_s - q$ are the surface-air differences in potential temperature and specific humidity, respectively; c_p is the specific heat capacity of air; and L_V is the latent heat of vaporization. The skill of the A87 scheme has been demonstrated previously using tower observations located over consolidated sea ice and snow (A87; Andreas, Horst, et al., 2010). Note that the A87 theoretical model was developed for exchange over uninterrupted ice and snow, as opposed to the mixture of ice floes and open water of the MIZ.

To represent scalar exchange over sea ice and the MIZ, numerical models have tended to adopt very simple approaches. For instance, contrary to the findings of A87, the MetUM and IFS schemes simply prescribe z_{0T} and z_{0q} as proportional to z_0 over uninterrupted sea ice, then use a *mosaic* technique similar to that expressed in Equation 1 to derive the exchange coefficients across the MIZ. See Lock and Edwards (2013), Renfrew, Elvidge and Edwards (2019) and Roberts et al. (2018) for details of the MIZ surface exchange schemes used in the MetUM and IFS, respectively. Lüpkes and Gryanik (2015) have presented a more complex parameterization framework for C_{HN} across the MIZ using a similar approach to that described above for C_{DN}; that is, including a component that accounts for scalar exchange due to ice floe edges. In their study, it is noted that $\frac{z_{0T}}{z_0}$ could be derived using existing parameterizations (including A87), though they do not implement this approach.

In this study, we investigate scalar exchange over sea ice using new aircraft-derived observations focused on the MIZ. At over 230 data points, we believe this is the largest scalar exchange data set currently available for the MIZ. We then develop a novel parameterization scheme to represent scalar exchange over the MIZ, *given* the momentum exchange, that could be easily implemented in NWP, climate or sea-ice models. Finally, we demonstrate that this new scheme is significantly more accurate than existing schemes.

2. Acquisition and Processing of Aircraft Observations From Over Arctic Marginal Sea Ice

The observations used for this study come from two Arctic field campaigns: The Aerosol-Cloud Coupling and Climate Interactions in the Arctic (ACCACIA) field campaign of 2013, with observations over the MIZ of the Barents Sea and Fram Strait around Svalbard (Elvidge et al., 2016); and the Iceland Greenland Seas Project (IGP) field campaign of 2018, with observations over the MIZ to the south-east of Greenland (Renfrew et al., 2019, 2021). All observations have been obtained using the British Antarctic Survey's instrumented DH6 Twin Otter research aircraft. For details of the aircraft instrumentation see Fiedler et al. (2010) and Renfrew et al. (2019, 2021).

In-situ fluxes of momentum, heat, and moisture have been derived from the aircraft observations along low-level (typically ~40 m) *flux-runs*, that are assumed to be within the atmospheric surface layer, using the eddy covariance technique. Surface exchange coefficients are then derived from these fluxes using the conventional atmospheric surface layer assumptions of constant fluxes and logarithmic vertical profiles of wind, temperature and specific humidity. For model parameterization development, these exchange coefficients have been derived at the standard 10-m reference height and corrected to neutral stratification using the Monin Obukhov length following Elvidge et al. (2016).

The data have undergone careful quality control to detect and discard those *flux-runs* for which the sampled turbulence is not homogenous. For details of the assumptions and procedures employed in deriving these quantities—including quality control—see Petersen and Renfrew (2009). An estimate of sea-ice concentration (or fraction) along each *flux-run* has been derived from surface albedo measurements following Elvidge et al. (2016). We have used a *flux-run* length of ~9 km, following Elvidge et al. (2016), that is similar to values used in other previous studies. In total, 303 flux runs were available for this study, of which 196 are from ACCACIA and 107 are from IGP. However, quality control reduces this number to 168 + 99, 154 + 88 and 159 + 74, for "good" quality ACCACIA + IGP data for momentum, heat, and moisture exchange respectively. All observations are located over, just upwind of, or just downwind of, the MIZ (Figure 1).

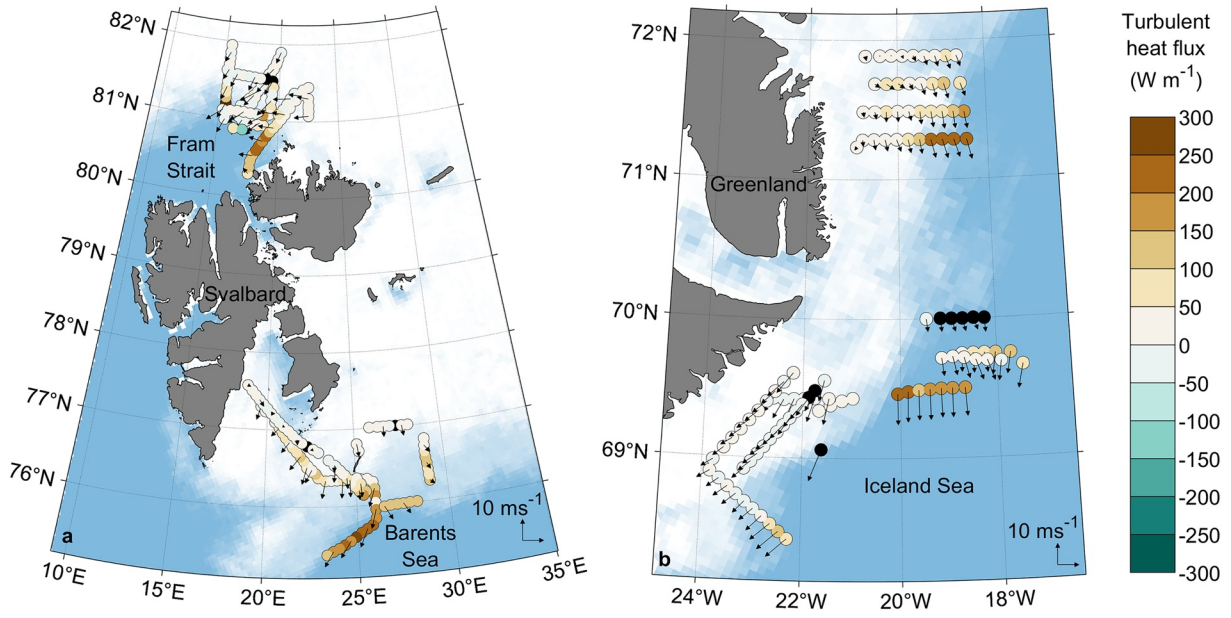

Figure 1. Spatial plots of all aircraft observations from the (a) ACCACIA and (b) IGP field campaigns showing total turbulent heat flux (color; positive values denoting upward fluxes) and wind vectors (arrows). Campaign-average sea-ice concentration is shown as blue-to-white shading. The wind vectors are scaled the same way for each panel and there are scale arrows in the bottom right corner of each panel. To aid clarity only one in three vectors are plotted in panel (a). Black dots show data points for which the turbulent heat flux is not available, either due to instrument failure (e.g., the five points along 70°N in panel (b), for which latent heat fluxes are not available) or failure to pass quality control.

3. Surface Fluxes of Heat and Moisture Under Cold Air Outbreak Conditions Across the Arctic MIZ

All observations used in this study were obtained under cold air outbreak conditions—that is, broadly northerly winds associated with predominantly upward and often large (up to 315 W m^{-2}) turbulent heat fluxes over and downwind of the MIZ as cool air sourced from high latitudes passes southwards over a relatively warm ocean (Figure 1). Across both field campaigns, for the observations over the sea just downwind of the MIZ, the interquartile ranges of SH and LH are 60–139 W m^{-2} and 34–64 W m^{-2}, respectively, both in the upward direction (not shown).

In Figure 2, SH and LH magnitudes ($|SH|$ and $|LH|$ respectively) and exchange coefficients for heat and moisture from all available data from each field campaign are presented, binned by sea-ice fraction (these bins are denoted hereafter as $bin_{A=x}$, where x is the ice fraction range). Generally, $|SH|$ and $|LH|$ are greatest over the sea and lower sea-ice fractions, and relatively small over higher ice fractions (Figures 2a–2d). This is due to the vertical gradients in temperature and humidity being much greater over the sea than over ice (see Equations 6 and 7). In contrast, the bin-median scalar exchange coefficients are smallest over the sea and greatest for the high ice fractions. For sensible heat exchange during ACCACIA, bin-median C_{HN} values increase monotonically with increasing ice fraction (Figure 2e). The median $|SH|$ for $bin_{A=1}$ is 11 Wm^{-2} (Figure 2a), which is modest but not insignificant. During IGP and for latent heat exchange during ACCACIA, the median exchange coefficient values peak over the MIZ at $bin_{A=0.75\text{-}1}$ (Figures 2f–2h) and median $|SH|$ and $|LH|$ for $bin_{A=1}$ are <4Wm^{-2} (Figures 2b–2d). Note such small fluxes increase the uncertainty in the C_{HN} and C_{EN} values derived from our observations. This may explain the relatively low median exchange coefficient values of $0.4–0.7 \times 10^{-3}$ for $bin_{A=1}$. On the other hand, these values are not inconsistent with the limited observations of scalar exchange available from previous studies. For example, Schröder et al. (2003) find $0.9 \pm 0.3 \times 10^{-3}$ for C_{HN} and $1.0 \pm 0.2 \times 10^{-3}$ for C_{EN} from 32 data points over a wide range of ice conditions; and Fiedler et al. (2010) find $0.7 \pm 0.1 \times 10^{-3}$ for C_{HN} from 20 data points over predominantly brash ice. More data is required to clarify whether or not C_{HN} and C_{EN} typically peak in the MIZ.

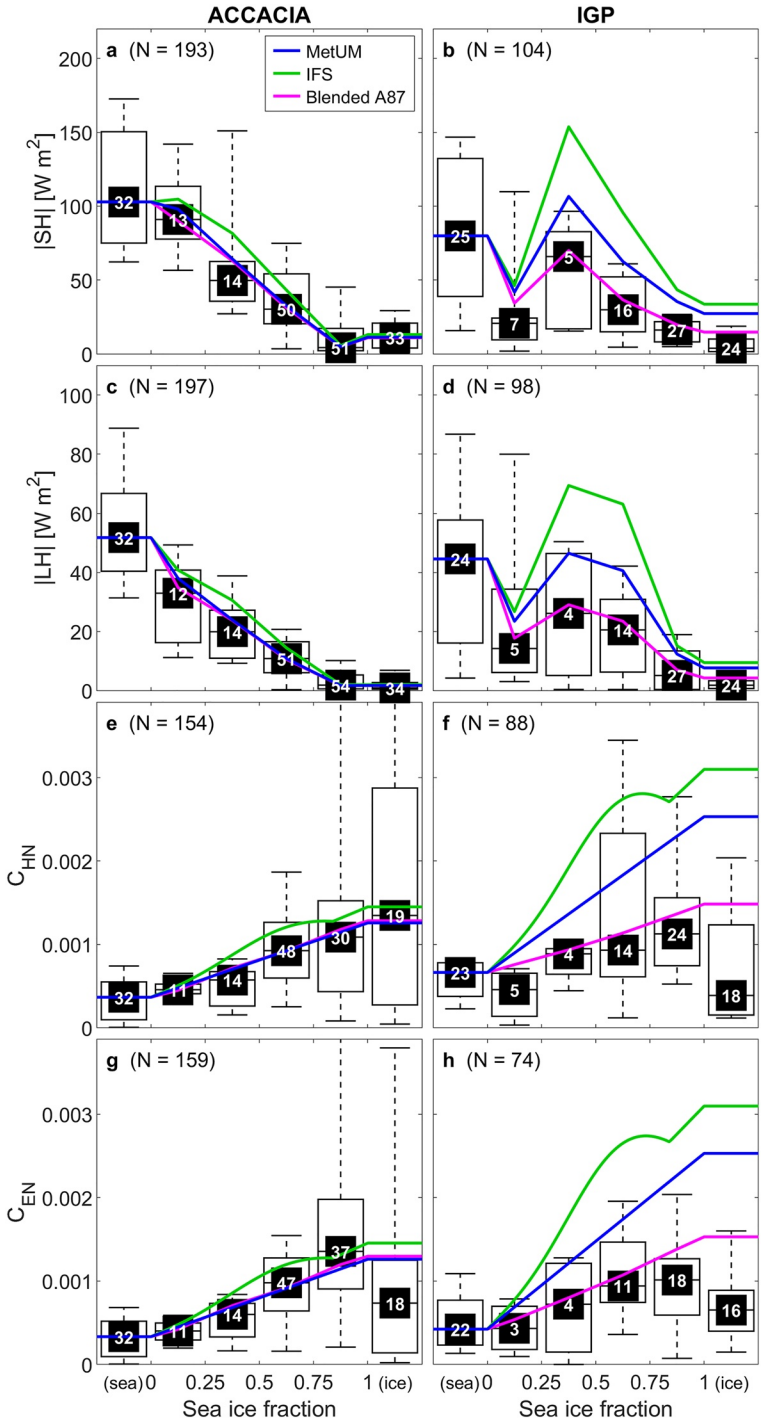

Figure 2. Turbulent heat flux magnitudes and exchange coefficients for heat and moisture as a function of ice fraction for all available observations from (left) the ACCACIA data set and (right) the IGP data set. Offline fluxes or exchange coefficients from the Met Office Unified Model (blue), IFS (green), and *Blended A87* (magenta) schemes are overlaid. All panels show observations as box and whiskers plots with the median (horizontal line), interquartile range (open box) and 10th and 90th percentiles (whiskers) for the following ice fraction bins: 0 ("sea"), 0–0.25, 0.25–0.5, 0.5–0.75, 0.75–1, and 1 ("ice"). The number of data points in each bin is shown at the median value. The ice fraction is based on the albedo as derived from aircraft observations of shortwave radiation. For the model schemes, for each field campaign, C_{HNw} and C_{ENw} (i.e., C_{HN} and C_{EN} in the sea bin) are set to the median observed values, and, in contrast to operational settings, z_{0i} (i.e., z_0 in the "ice" bin; used in the derivation of $C\mathrm{HN}_i$ and $C\mathrm{EN}_i$) is also set to the median observed value. For each panel, the total number of data points plotted (N) is given.

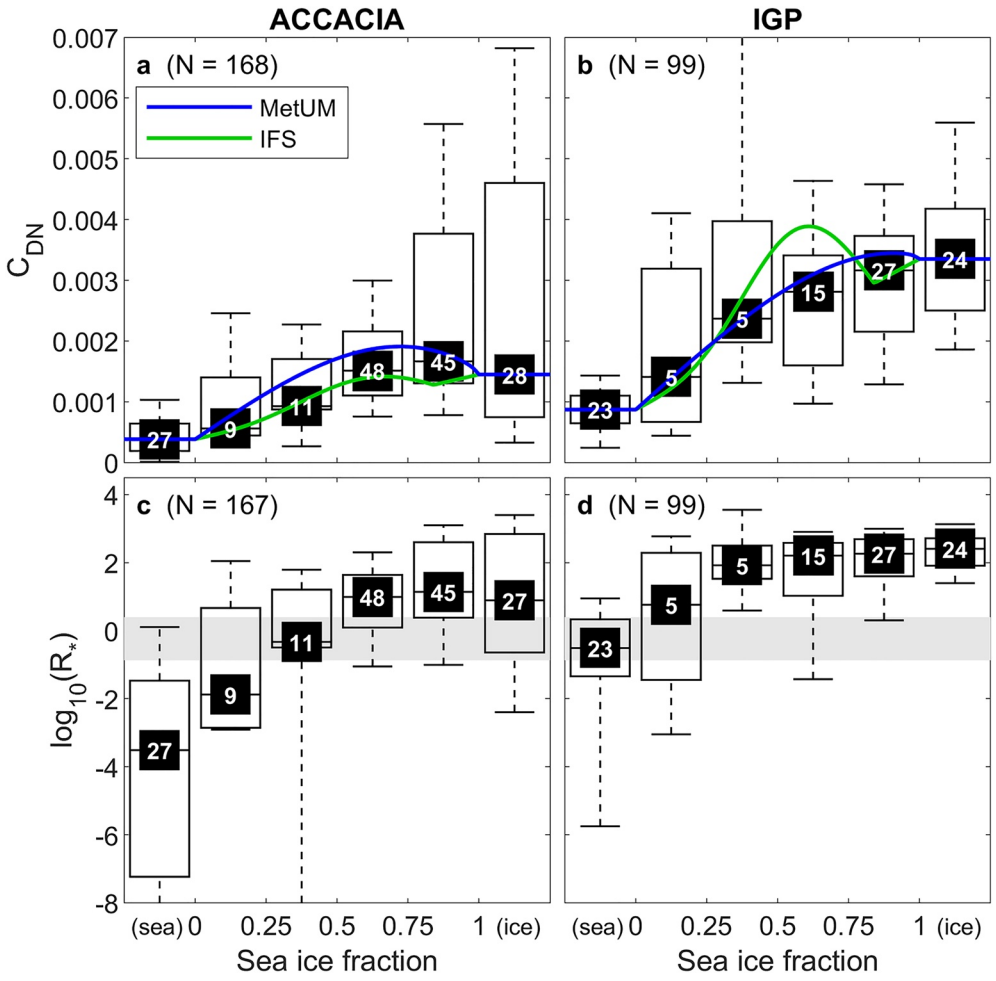

Figure 3. Drag coefficient, C_{DN}, and roughness Reynolds number, $\log_{10}(R_*)$, as a function of ice fraction for observations from (a and c) the ACCACIA data set and (b and d) the IGP data set. All panels show observations as box and whiskers plots with the median, interquartile range and 10th/90th percentiles (following Figure 2). Algorithms from the Met Office Unified Model (blue) and Integrated Forecast System (green) are shown in (a and b), with C_{DNw} and C_{DNi} anchored to observations. For each panel, the total number of data points plotted (N) are given. In (c and d), gray background shading marks the *transitional* aerodynamic roughness regime, below which ($R_* < 0.135$) is the *smooth* regime, and above which ($R_* > 2.5$) is the *rough* regime.

4. The Parameterization of Surface Heat and Moisture Exchange Over Uninterrupted Sea Ice

The parameterization of surface heat and moisture exchange is dependent on that of surface momentum exchange, since C_{HN} and C_{EN} are functions of z_0 (see Equations 4 and 5). Figures 3a and 3b show observed C_{DN} across the MIZ (in the same format as Figure 2). In the ACCACIA data, median C_{DN} exhibits a peak over the MIZ, at $\text{bin}_{A = 0.75\text{-}1}$, in agreement with previous studies (see Section 1). In the IGP data however, median C_{DN} rises monotonically with ice fraction to peak over uninterrupted sea ice. Furthermore, the median C_{DN} (and consequently z_0) is systematically larger in the IGP data than in the ACCACIA data. For ACCACIA and IGP, the median observed z_{0i} are 4.3×10^{-4} m and 10^{-2} m, respectively. To put these values in context, and to highlight the relative roughness of the ice observed during the IGP campaign, a one-year record of tower observations from the Arctic yielded a median z_{0i} of 3–6 $\times 10^{-4}$ m (the precise value being dependent on the sensor height) (Persson et al., 2002). Owing to the higher z_0 and also stronger windspeeds (see Figure 1), the roughness Reynolds number R_* is consistently greater in the IGP data set than in the ACCACIA data set for all ice-fraction bins (cf. Figures 3c and 3d). In other words, the IGP surface flow regime

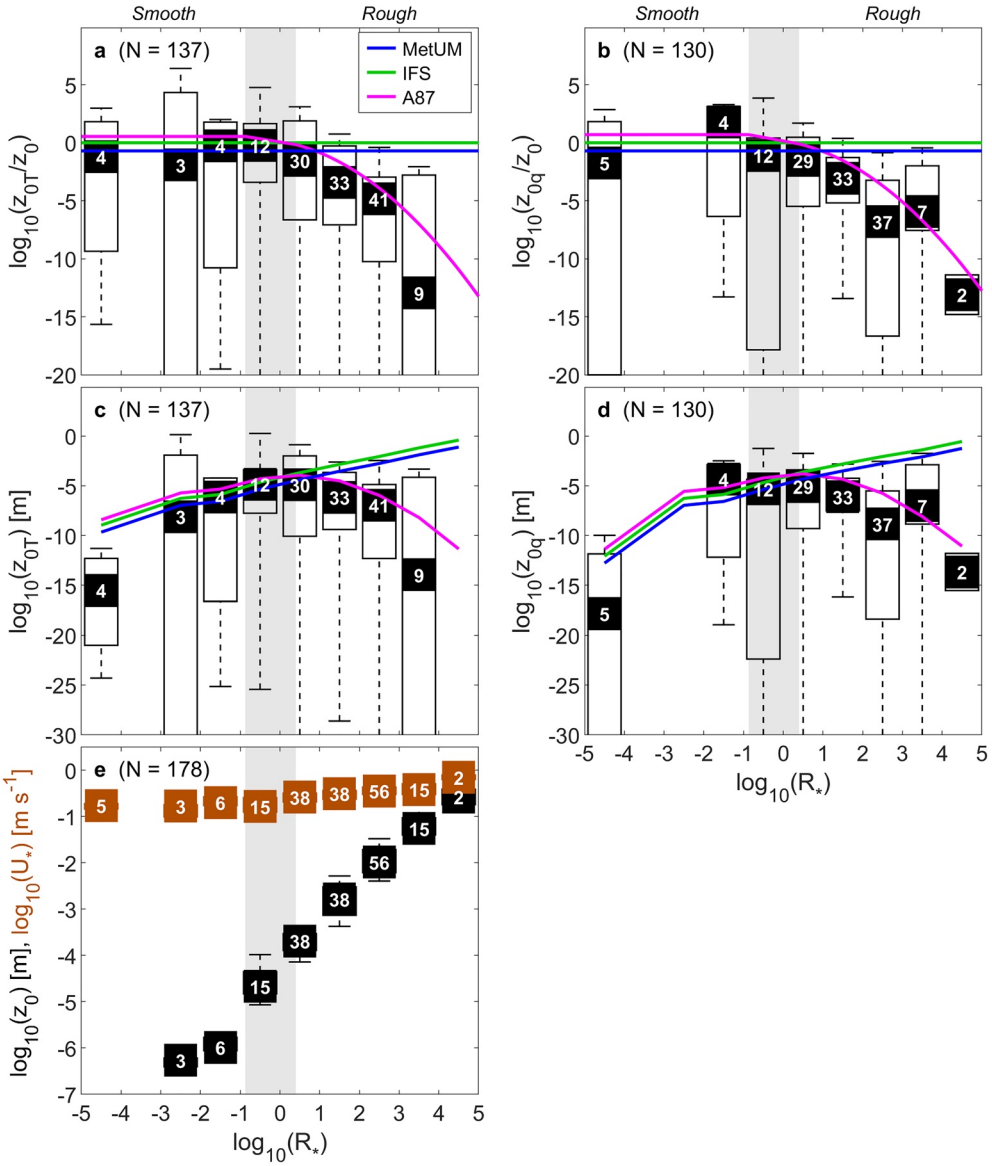

Figure 4. Relationships between surface roughness characteristics and R_* from aircraft-derived observations over the marginal ice zone and the functional form of scalar flux algorithms over sea ice. Panels show (a) $\log_{10}(z_{0T}/z_0)$, (b) $\log_{10}(z_{0q}/z_0)$, (c) $\log_{10}(z_{0T})$, (d) $\log_{10}(z_{0q})$, and (e) $\log_{10}(u_*)$ in brown and $\log_{10}(z_0)$ in black versus $\log_{10}(R_*)$, for all observations where ice fraction is > 0.5 from both the ACCACIA and IGP field campaigns. Overlaid in (a–d) are the parameterizations from the Met Office Unified Model (MetUM), Integrated Forecast System (IFS) and A87. The observations are shown as box and whiskers with the median, interquartile range and 10th and 90th percentiles (following Figure 2). Gray background shading marks the *transitional* aerodynamic roughness regime, to the left of which ($R_* < 0.135$) is the *smooth* regime, and to the right of which ($R_* > 2.5$) is the *rough* regime. For each panel, the total number of data points plotted (N) are given. Note quality control leads to fewer data points in panels (a–d) compared to panel (e). Note that the MetUM and IFS schemes have, respectively, $z_{0T}/z_0 = z_{0q}/z_0 = 0.2$ and $z_{0T}/z_0 = z_{0q}/z_0 = 1$.

is aerodynamically rougher. Note that in contrast to C_{DN}, there is no such systematic difference between the two field campaigns in either C_{HN} or C_{EN} (cf. Figures 2e–2h).

Figures 4a and 4b show z_{0T}/z_0 and z_{0q}/z_0 plotted against R_* (replicating Figure 8 from A87), with the addition of our observations, binned by R_*. The A87 theoretical model is plotted and the three aerodynamical regimes—*smooth*, *transitional* and *rough*—are indicated. Since the A87 scheme is for snow and ice, only

those observations with ice fractions greater than 0.5 are used here. The observations broadly follow the line predicted by the A87 scheme, with z_{0T}/z_0 and z_{0q}/z_0 being broadly insensitive to R_* in the *smooth* regime and decreasing exponentially with increasing R_* in the *rough* regime.

Figures 4c–4e show z_{0T}, z_{0q} and z_0, respectively, as functions of R_*. Our observations show that z_0 increases monotonically with R_*, whilst z_{0T} and $z_{0q}$are broadly positively correlated with R_* in the *smooth* regime, and negatively correlated with R_* in the *rough* regime (i.e., with a peak around the *transitional* regime). This result is predicted by the A87 theoretical model, but, as far as we are aware, it has never been demonstrated in observations. Our observations also show that R_* is a much stronger function of z_0 than it is of u_*, as z_0 varies by many orders of magnitude with R_*, while u_* only varies by about 1 order of magnitude (Figure 4e). R_* is a comparatively weak function of ν.

The differing sensitivities to R_* of the roughness lengths for momentum and for the scalars can be explained physically within the framework of the A87 model. In the smooth regime, roughness elements are embedded in the viscous sublayer and only skin friction is present. Turbulent eddies remain in motion as they scour the ice/snow surface, transferring scalar constituents across the interface by advective diffusion. The absence of form drag means that the *Reynolds Analogy* holds: that is, both momentum and heat transfer depend on the same turbulent eddies, and so z_{0T}/z_0 and z_{0q}/z_0 are constant. In the rough regime, eddies in contact with the surface become stagnant—trapped by roughness elements that extend above the viscous sublayer—and scalar transfer is strictly a diffusion process. Here, momentum exchange is due to both skin friction within the viscous sublayer and form drag above. The addition of pressure forces means the *Reynolds Analogy* is no longer valid, and momentum exchange is enhanced relative to heat exchange. Consequently, z_{0T}/z_0 and z_{0q}/z_0 decrease as aerodynamic roughness—and consequently the influence of pressure forces—increases.

Previous studies have highlighted that self-correlation due to the same values of z_0 and u_* appearing in both x and y axes of plots such as those in Figure 4 can generate a fictitious correlation (e.g., Andreas, 2002; Andreas, Horst, et al., 2010). To avoid this issue, those studies have derived R_* using a bulk parameterization. In Appendix A, we explain why this approach is not appropriate here, and show that self-correlation, whilst present, does not significantly affect our results. Note that the relationships shown in Figures 4a–4d are not significantly affected by varying the ice fraction threshold used to select the data from 0.5 to 0.75. However, as the threshold increases, the number of data points reduces and the scatter increases.

5. Validation of Existing Model Parameterizations of Scalar Exchange in the MIZ

In Figures 2 and 3, the MIZ surface exchange parameterization schemes used in the MetUM and IFS are plotted over the observations. Since our focus here is exchange over sea ice and the MIZ, for each field campaign we have fixed the exchange coefficients over open water (C_{DNw}, C_{HNw} and C_{ENw}) and the equivalent roughness lengths (z_{0w}, z_{0Tw}, and z_{0qw}) in the parameterization schemes to the median observed values. Likewise, since our concern is scalar as opposed to momentum transfer, we have also fixed C_{DN}, z_0 to the median observed values at an ice fraction of 1. That is, we prescribe an accurate representation of C_{DNi} (or z_{0i}), where subscript i denotes uninterrupted sea ice. The MetUM and IFS schemes use z_{0i}, z_{0Ti}, z_{0qi} and Equations 4 and 5 to derive C_{HNi} and C_{ENi}. The scalar roughness lengths are defined as $z_{0Ti} = z_{0qi} = 0.2\, z_{0i}$ in the MetUM, and $z_{0Ti} = z_{0qi} = z_{0i}$ in the IFS. The scalar exchange coefficients across the MIZ are then given by:

$$C_{\mathrm{HN}} = \left(1 - A\right) C_{\mathrm{HNw}} + A\, C_{\mathrm{HNi}}, \tag{8}$$

$$C_{\mathrm{EN}} = \left(1 - A\right) C_{\mathrm{ENw}} + A\, C_{\mathrm{ENi}}. \tag{9}$$

Here, these coefficients are used to derive the *offline* parameterized heat fluxes shown in Figures 2a–2d using observed ρ, U, θ, θ_s, q, and q_s, and Equations 6 and 7. Note that these *offline* fluxes are derived using *flux-run* averaged surface temperatures—not using the *mosaic* approach applied when these schemes are implemented in a NWP model. This is necessary since extracting separate sea ice and open water values for surface temperature and humidity from our observations over the MIZ is not generally possible, due to differences in the measurement area (or "footprint") of the aircraft-mounted instruments used to derive

ice fraction and surface temperature. Our approach allows an evaluation of the relative performance of the different schemes, given the differences in the exchange coefficients they predict.

For both field campaigns, the MetUM and IFS schemes accurately reproduce the variability in C_{DN} with ice fraction across the MIZ when C_{DNw} and C_{DNi} are fixed to the observations (Figures 3a and 3b). For the ACCACIA data, they also provide a relatively good representation of scalar exchange, with the MetUM performing better than the IFS: the MetUM (IFS) scheme exhibits positive biases in bin-median $\left|\mathrm{SH}\right|$ and $\left|\mathrm{LH}\right|$, peaking at 13 (31) and 4 (11) W m^{-2}, respectively (Figures 2a, 2c, 2e, and 2g). For the IGP data, the schemes significantly overestimate scalar exchange across the MIZ (Figures 2b, 2d, 2f, and 2h). Biases in the exchange coefficients increase with ice fraction, peaking for $\mathrm{bin}_{A=1}$ where bin-median values are several times greater than observed. Biases in the heat fluxes are greatest at intermediate ice fractions, with bin-median biases for the MetUM (IFS) in $\left|\mathrm{SH}\right|$ and $\left|\mathrm{LH}\right|$ reaching 41 (88) and 20 (43) W m^{-2}, respectively, for $\mathrm{bin}_{A=0.25\text{-}0.5}$. Flux biases are smaller at the higher ice fractions, despite larger biases in the exchange coefficients, because the fluxes are much smaller.

The consistently larger bias in the IFS scheme relative to the MetUM scheme reflects the fact that $\frac{z_{0T}}{z_0} = \frac{z_{0q}}{z_0} = 1$ (used in the former) is, on the whole, a worse match than $\frac{z_{0T}}{z_0} = \frac{z_{0q}}{z_0} = 0.2$ (used in the latter) to our observations (Figures 4a and 4b). It is however evident that in aerodynamically smooth ice ($\log_{10}\left(R_{*i}\right) < 0.5$), the A87 model predicts a value of k that is in fact closer to that used in the IFS than the MetUM scheme. So in certain conditions, the IFS scheme may be expected to perform better than the MetUM scheme.

The reason for the disparity in performance of the existing model parameterization schemes between the two field campaigns is apparent from Figure 4. Over uninterrupted sea ice, these schemes have z_{0T} and z_{0q} proportional to z_0. This is broadly consistent with our observations and the theoretical model of A87 in the *smooth* regime, but fails to capture the observed decrease in z_{0T} and z_{0q} with increasing R_* in the *rough* regime. In contrast, the A87 model does capture this behavior. Consequently, in the reproduction of heat and moisture exchange across the MIZ (Figure 2), all three schemes perform well for the comparatively aerodynamically smooth conditions observed during ACCACIA (characterized by a median $\log_{10}\left(R_{*i}\right)$ of ~1; Figure 3c), whilst only the A87 model performs well for the aerodynamically rougher conditions observed during IGP (characterized by a median $\log_{10}\left(R_{*}\right)$ of ~2.5; Figure 3d). Our observations confirm A87's theoretical model, demonstrating the dependence of the relationship between momentum exchange and scalar exchange on aerodynamic roughness. This suggests that surface exchange parameterization schemes for the MIZ could be improved if they were to represent this dependency. In Section 6 we derive and test such a scheme.

6. Derivation and Validation of a New, Aerodynamic-Roughness-Dependent Scalar Exchange Parameterization for the MIZ

Since the A87 theoretical model is only appropriate over sea ice, to provide a useful prediction of scalar exchange across the MIZ we propose a new parameterization approach, based on blending the A87 scheme with an ocean exchange scheme. Our scheme provides the exchange coefficient for heat, blended across the MIZ, as follows:

$$z_{0Ti} = z_{0i}\, f\left(R_{*i}\right), \tag{10}$$

$$C_{\mathrm{HNi}} = \frac{\kappa^2}{\ln\left(z \,/\, z_{0i}\right)\ln\left(z \,/\, z_{0Ti}\right)}, \tag{11}$$

$$C_{\mathrm{HN}} = \left(1 - A\right)C_{\mathrm{HNw}} + A\, C_{\mathrm{HNi}}, \tag{12}$$

where R_{*i} is R_* over uninterrupted sea ice, and $f\left(R_{*i}\right)$ denotes the A87 scheme for deriving $\frac{z_{0Ti}}{z_{0i}}$ from R_{*i} (i.e., the pink line in Figure 4a). An analogous set of equations can be defined for moisture exchange. Note that in the A87 theoretical model, the derivations for heat and moisture differ slightly the derivations for heat and moisture differ slightly (i.e., the relationship given by the pink line in Figure 4a differs slightly from that in Figure 4b). Note that R_{*i} is distinct from R_* as presented in Figures 3c and 3d, since the observations used for these figures are for a range of ice fractions.

We validate this *Blended A87* scheme against our observations using a similar approach to that used for validating the MetUM and IFS schemes in Section 5. Again, z_{0i}, z_{0w}, z_{0Tw}, and z_{0qw} are set to the median observed values for each field campaign. We also require R_{*i}, which is derived from turbulence observations for each *flux-run* using an adapted version of Equation 2, as follows:

$$R_{*i} = \frac{z_{0i}\, u_{*i}}{\nu}, \tag{13}$$

$$u_{*i} = \frac{-\kappa U}{\ln\left(z_{0i} / z\right) + \varphi}, \tag{14}$$

where ν is kinematic viscosity, derived from observed air temperature and density using Sutherland's formula (see for example Burnett, 1965); φ is a stability correction function (see for example Stull, 1988); and $z = 10\,m$. In this context, for each *flux-run*, R_{*i} denotes R_* over any sea ice and, for each field campaign, R_{*i} varies predominantly with U (but also with φ and, negligibly, with ν). U, φ, and ν are all taken from our observations. For heat exchange, Equations 10 and 11 are then used to determine C_{HNi}, which is combined with C_{HNw} using Equation 12 to provide a *Blended A87* value of C_{HN} for each *flux-run*. Again, using analogous equations, the same procedure applies for deriving C_{EN}. To compare against observations, the C_{HN} and C_{EN} values are binned by ice fraction and the bin-median heat fluxes (pink lines in Figure 2a–2d) are derived in the same manner as for the MetUM and IFS schemes (see Section 5).

Note that implementation of the *Blended A87* scheme in an NWP model would be straightforward, since z_{0w}, z_{0Tw}, and z_{0qw} would be provided by the model's ocean surface exchange scheme; and A, z_{0i} and u_{*i} would be provided by the model's MIZ surface momentum exchange scheme. In this context, for each grid box, R_{*i} would denote R_* over any sea ice and would vary with U, φ, ν and, if variable in the model, z_{0i}. Recall however that z_{0i} is currently fixed in most weather and climate models.

Unlike the MetUM and IFS schemes, the *Blended A87* scheme, run offline, reproduces scalar exchange reasonably accurately for the IGP field campaign (Figure 2), except for an overestimate for $\mathrm{bin}_{A=1}$ (though this overestimate is much smaller than those in the MetUM and IFS schemes, and recall from Section 3 that there is some uncertainty in the observed exchange coefficients in $\mathrm{bin}_{A=1}$). With respect to key statistics, the *Blended A87* scheme performs much better in the reproduction of SH and LH for IGP (Table 1; Figure 5), whilst more modest improvements are seen for ACCACIA (Table 1). For IGP, the bias error (root mean square error; R.M.S. error) in total turbulent heat flux for the *Blended A87* scheme is 13 (25) W m^{-2}; which is considerably lower than the equivalent errors of 48 (63) W m^{-2} and 80 (103) W m^{-2} found for the MetUM and IFS schemes, respectively. For ACCACIA, the bias error (R.M.S. error) in total turbulent heat flux for the *Blended A87* scheme is 0 (29) W m^{-2}; marginally lower than the equivalent error of 3 (33) W m^{-2} found for the MetUM scheme and significantly lower than the 17 (49) W m^{-2} found for the IFS scheme.

The large improvement seen for the IGP data is due to the new scheme being sensitive to aerodynamic roughness via R_{*i} (i.e., predominantly z_{0i} and U), whilst the MetUM and IFS schemes are not. Note that in the ACCACIA data there is little difference in the representation of C_{HNi} and C_{ENi} (and consequently also z_{0Ti} and z_{0qi}) in each of the schemes (see Figures 2e and 2g). The more modest improvement in the *Blended A87* scheme here is predominantly due to its sensitivity to variability in U across the MIZ, and also possibly to more accurate values of z_{0T}/z_0 and z_{0q}/z_0 at average wind speeds.

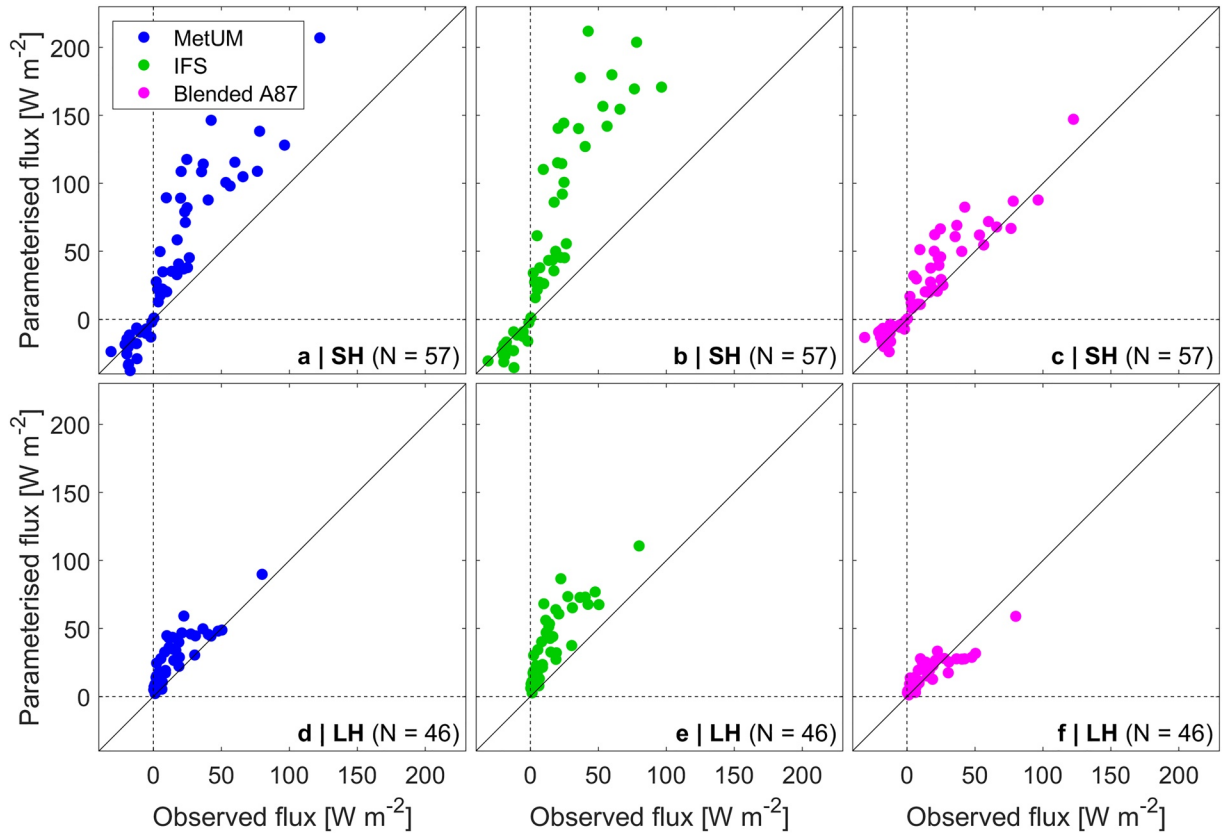

Figure 5. Scatter plots of (a–c) sensible heat flux and (d–f) latent heat flux for the IGP data set. Observations are derived from the aircraft data using the eddy covariance technique; model estimates are calculated offline from the (a and d) Met Office Unified Model, (b and e) Integrated Forecast System and (c and f) *Blended A87* schemes. For each panel, the total number of data points plotted (*N*) are given. Data points over open water (ice fraction of 0) and where the observed surface exchange coefficients are anomalously small (below the 10th percentile) are excluded.

7. Conclusions

This study has presented aircraft observations from two field campaigns in the Arctic, amounting to an observational data set of unprecedented spatial coverage, for the study of scalar exchange over sea ice and the MIZ. Our observations show large turbulent heat and moisture fluxes over and downwind of the MIZ during cold air outbreak conditions. They corroborate previous studies in showing that scalar exchange varies with ice fraction, surface roughness and wind speed. Where the surface roughness is small relative to the viscous length-scale of the flow (relatively weak winds over smooth sea ice), the roughness Reynolds number (R_*) is small, that is, conditions are aerodynamically *smooth*. In such conditions over uninterrupted sea ice, the surface roughness lengths for heat and moisture can be accurately described as being proportional to the surface roughness length for momentum, as is prescribed in the parameterization schemes currently used in two state-of-the-art NWP models—the MetUM and IFS. These schemes therefore have the potential to perform relatively well for aerodynamically *smooth* conditions such as those observed during the ACCACIA field campaign.

However, our observations have revealed that in an aerodynamically *rough* regime (relatively strong winds over rough sea ice), the scalar roughness lengths are inversely correlated with the roughness length for momentum. Consequently, scalar roughness lengths peak in the *transition* between the *smooth* and *rough* regimes—a finding that, as far as we are aware, has not previously been demonstrated. In the aerodynamically *rough* sea ice regime—such as observed during the IGP field campaign—the MetUM and IFS parameterization schemes are not suitable and become ever less so with increasing R_*. For the IGP data, this leads to overestimates in the median sensible and latent heat fluxes of up to 40 and 22 W m^{-2}, respectively, in offline tests.

Table 1
Parameterisation Performance Statistics for Heat Fluxes Using Data From the ACCACIA and IGP Field Campaigns

		ACCACIA			IGP		
Heat flux	Attribute	MetUM	IFS	Blended A87	MetUM	IFS	Blended A87
Sensible	Bias error (W m^{-2})	2.9	12.0	**0.5**	25.2	39.7	**10.2**
	R.M.S. error (W m^{-2})	27.1	39.7	**23.5**	40.5	65.0	**16.4**
	Correlation coefficient	0.83	0.81	**0.84**	0.91	0.91	**0.93**
Latent	Bias error (W m^{-2})	**0.1**	2.9	-0.3	12.3	22.0	**1.2**
	R.M.S. error (W m^{-2})	6.6	9.2	**6.4**	15.7	26.8	**8.6**
	Correlation coefficient	**0.86**	0.84	**0.86**	0.85	0.84	**0.87**
Turbulent	Bias error (W m^{-2})	3.1	16.6	**0.0**	48.3	80.5	**13.1**
	R.M.S. error (W m^{-2})	32.7	49.3	**28.9**	62.6	103.4	**24.7**
	Correlation coefficient	**0.84**	0.81	**0.84**	0.87	0.87	**0.90**

Note. The data used to derive these statistics are from aircraft measurements and offline experiments in the MetUM, IFS and *Blended A87* schemes. The bias, root-mean-square (R.M.S.) error and correlation coefficient from a linear regression are shown. Blue shading indicates which of the three schemes performs best in each statistic for each field campaign. For ACCACIA (IGP), there are 103 (57), 104 (46), and 90 (38) data points used respectively for sensible, latent and turbulent (sensible + latent) heat flux statistics. Data points over open water (ice fraction of 0) and where the observed surface exchange coefficients are anomalously small (below the 10th percentile) are excluded.

In contrast, the theoretical model of A87 for scalar exchange over uninterrupted sea ice does predict the key relationships between the scalar roughness lengths and R_* from our observations over high ice concentrations. Consequently, we have derived a simple new parameterization scheme for scalar exchange across the MIZ by blending output from the A87 model with air-sea exchange as a function of ice fraction. Due to the sensitivity of this new scheme to surface roughness and wind speed, it performs significantly better than the MetUM and IFS schemes for the IGP field campaign, more than halving the bias and R.M.S. errors in total turbulent heat flux in offline tests. The new scheme also performs slightly better for the ACCACIA field campaign, due to its sensitivity to wind speed and possibly more accurate values of z_{0T}/z_0 and z_{0q}/z_0 at average wind speeds. Our *Blended A87* scheme is more consistent with surface-renewal theory and, according to our observations, provides a more physically realistic treatment of scalar exchange over the MIZ than the existing, operational NWP schemes.

There is a large amount of scatter in our observations, as is expected for measurements of turbulence from a limited aircraft-derived data set. Furthermore, our results are limited to off-ice flow in predominantly statically unstable conditions. Consequently, additional observations in different regions and under different meteorological conditions would be useful in corroborating our findings and testing the veracity of our proposed parameterization. Further testing of the *Blended A87* scheme is required using different observational data sets. For example, measurements from a ship would complement our aircraft measurements and, owing to the higher spatial resolution of such measurements, could enable the use of the *mosaic* approach for the offline derivation of parameterized surface fluxes. Recall that this *mosaic* approach would be applied if the scheme were implemented in an NWP model, but is inappropriate in offline experiments forced by aircraft observations such as those of the present study (see Section 5).

While our new scheme demonstrates the importance of incorporating sensitivity to aerodynamic roughness over uninterrupted sea ice (via R_{*i}) in the parameterization of scalar exchange over the MIZ, it does not incorporate the effects of ice floe edges. The scheme proposed in Lüpkes and Gryanik (2015) does incorporate these effects via a scalar exchange component similar to the form drag component used for momentum exchange (see Section 1). Their scheme predicts peaks in the scalar exchange coefficients over the MIZ. Our observations support such peaks in three of four cases. However these observed peaks are a result of exchange coefficient values for an ice fraction of 1 that are much smaller than predicted by the A87 model and may be unphysical (see Section 3). Further work is required to verify the physical basis for the incorporation of ice floe edge effects in scalar exchange parameterization.

It is important to note the skill of the new scheme is dependent on an accurate representation of the sea ice topography (i.e., z_{0i}), since R_{*i} is a strong function of z_{0i}. This study corroborates previous work in showing that z_{0i} varies considerably with region. This variability is a function of several factors including sea-ice type, age, and thickness; and deformation and erosion by wind, waves, and water drainage. It is currently not clear how to represent this variability in models, so existing parameterization schemes usually prescribe a fixed z_{0i}. This is a major limitation to progress in this field that will require significant further research to address. For example, Elvidge et al. (2016) discuss the possibilities of using sea-ice model output, satellite-derived roughness estimates (Petty et al., 2017) or a stochastic element to sea-ice drag parameterization. The representation of scalar exchange over the MIZ would also benefit from improved model representation of surface roughness over water surfaces within the MIZ (i.e., C_{z0w}). This is currently typically provided by a model's ocean exchange scheme via some form of Charnock's relation (Charnock, 1955), which is most appropriate for open ocean conditions and less applicable in the MIZ, where the presence of sea ice means that waves are generally dampened relative to in the open ocean, suggesting a fetch dependence may be worth investigating in future work.

Surface fluxes of heat and moisture in the MIZ are known to impact the weather and climate of the high latitudes and the development of weather systems downwind, for example, over Northern Europe (Renfrew, Elvidge, & Edwards, 2019). The volume and spatial coverage of sea ice and marginal ice in the Polar oceans are changing; the MIZ is widening whilst total sea-ice coverage is reducing (Strong & Rigor, 2013). These trends are expected to continue in the future (Sigmond et al., 2018). The potential impacts of these changes on the atmosphere are poorly understood as our current capacity to model the variability in air-sea-ice exchanges in the polar regions is lacking. New shipping routes resulting from these changes will also require improved weather forecasts across the Arctic Ocean. Consequently, there is strong motivation to improve the representation of surface fluxes of heat and moisture over sea ice in weather and climate models. The scheme we have developed provides a straightforward framework for doing so, though improved representation of z_{0i} will be necessary to reap its full benefit.

Appendix A: Significance of Self-Correlation in Our Validation of the A87 Scheme

In Figures 4a and 4b, the same z_0 values, derived from aircraft turbulence observations, appear in both the x-axes ($R_* = \frac{z_0\, u_*}{\nu}$) and the y-axes (z_{0T}/z_0 and z_{0q}/z_0). Furthermore, u_* appears in z_0, z_{0T}, z_{0q} and R_*, with the roughness lengths derived from our observations as follows,

$$z_0 = z\, exp\left\{-\kappa \frac{U}{u_*} - \varphi\right\},$$

$$z_{0T} = z\, exp\left\{-\kappa \frac{\theta - \theta_s}{\theta_*} - \varphi_S\right\},$$

$$z_{0q} = z\, exp\left\{-\kappa \frac{q - q_s}{q_*} - \varphi_S\right\},$$

where $\theta_* = \frac{-\overline{w'\theta'}}{u_*}$; $q_* = \frac{-\overline{w'q'}}{u_*}$; w', θ' and q' are perturbations in vertical wind component, potential temperature and specific humidity, respectively; and φ_S is a stability correction function for heat and moisture. This means there will be a degree of self-correlation in these plots; and this will affect our validation of the A87 scheme. Previous studies (Andreas, 2002; Andreas, Horst, et al., 2010; Andreas, Persson, et al., 2010) have avoided this self-correlation by deriving R_* from observations using bulk parameterization. Whilst this approach is suitable for testing a bulk flux scheme, it would be inappropriate for this study, which aims to improve the representation of surface heat and moisture exchange, *given* the momentum exchange.

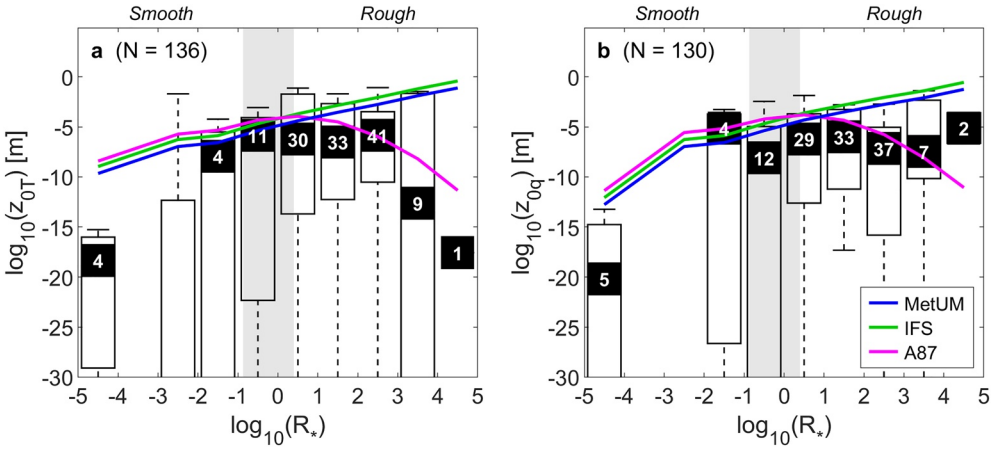

Figure A1. As Figures 4c and 4d, but with the observed u_* in z_{0T} and z_{0q} replaced with a fixed value of 0.3 (the median of the observed values). The lines showing the parameterization schemes are unchanged from Figures 4c and 4d and are plotted to aid comparison.

Note also that the accuracy of z_{0i} derived from bulk parameterization is limited; we have confirmed this by comparing z_{0i} derived from our observations using eddy covariance with those using the Andreas, Horst, et al. (2010) bulk parameterization—the correspondence is weak (not shown). Consequently, in this study we have tested the parameterization of z_{0T} and z_{0q}, *given* z_{0i} (and consequently R_{*i}) from our turbulence observations. We now assess the impact of self-correlation on these tests.

The fact that z_{0T} and z_{0q} exhibit sensitivities to R_* which are strong, similar, physically consistent with theory (see Section 4), and greater than that exhibited by z_0 (Figures 4c–4e) demonstrates that the self-correlation due to z_0 does not dominate the sensitivity of z_{0T}/z_0 or z_{0q}/z_0 to R_*. In Figure A1, the observed values of u_* used in the derivation of z_{0T} and z_{0q} (y-axis) have been replaced with a fixed value of 0.3 (the median of the real, observed values). The resultant relationships are almost identical to those shown in Figures 4c and 4d. That is, broadly increasing z_{0T} and z_{0q} with R_* in the *smooth* regime, and decreasing z_{0T} and z_{0q} with R_* in the *rough* regime. This demonstrates that the influence of u_* on the variability of each of z_{0T} and z_{0q} with R_* is relatively weak. In Figure A1b, z_{0qi}/z_{0i} in the largest R_* bin ($4 < R_* \leq 5$) is a notable outlier; however there are only two data points in this bin, so its significance is small.

We conclude therefore that the use of R_* derived from our turbulence observations over sea ice to validate and develop scalar exchange parameterization schemes is justified, as self-correlation, whilst present, does not significantly impact our results.

Acknowledgments
This paper was made possible by funding provided by NERC under the project grants '*Atmospheric Forcing of the Iceland Sea*' (NE/N009754/1) and '*Candiflos*' (NE/S000453/1 and NE/S000690/1). We acknowledge all participants of the ACCACIA and IGP field campaigns who contributed to obtaining the aircraft observations used for this study. We thank Christof Lüpkes and two anonymous reviewers for their comments, which led to significant improvements in the paper. This study is a contribution to the Year of Polar Prediction (YOPP), a flagship activity of the Polar Prediction Project, initiated by the World Weather Research Programme of the World Meteorological Organisation.

Data Availability Statement

The data used for this study are available on CEDA via British Antarctic Survey (2014) for the MASIN observations from ACCACIA, and via Renfrew (2019) for the MASIN observations from IGP.

References

Andreas, E. L. (1987). A theory for the scalar roughness and the scalar transfer coefficients over snow and sea ice. *Boundary-Layer Meteorology*, *38*(1–2), 159–184. https://doi.org/10.1007/bf00121562

Andreas, E. L. (2002). Parameterizing scalar transfer over snow and ice: A review. *Journal of Hydrometeorology*, *3*(4), 417–432. https://doi.org/10.1175/1525-7541(2002)003<0417:pstosa>2.0.co;2

Andreas, E. L., Horst, T. W., Grachev, A. A., Persson, P. O. G., Fairall, C. W., Guest, P. S., & Jordan, R. E. (2010). Parametrizing turbulent exchange over summer sea ice and the marginal ice zone. *Quarterly Journal of the Royal Meteorological Society*, *136*(649), 927–943. https://doi.org/10.1002/qj.618

Andreas, E. L., Persson, P. O. G., Grachev, A. A., Jordan, R. E., Horst, T. W., Guest, P. S., & Fairall, C. W. (2010). Parameterizing turbulent exchange over sea ice in winter. *Journal of Hydrometeorology*, *11*(1), 87–104. https://doi.org/10.1175/2009jhm1102.1

Arya, S. P. S. (1973). Contribution of form drag on pressure ridges to the air stress on Arctic ice. *Journal of Geophysical Research*, *78*(30), 7092–7099. https://doi.org/10.1029/jc078i030p07092

Arya, S. P. S. (1975). A drag partition theory for determining the large-scale roughness parameter and wind stress on the Arctic pack ice. *Journal of Geophysical Research*, *80*(24), 3447–3454. https://doi.org/10.1029/jc080i024p03447

Birnbaum, G., & Lüpkes, C. (2002). A new parameterization of surface drag in the marginal sea ice zone. *Tellus A: Dynamic Meteorology and Oceanography*, *54*(1), 107–123. https://doi.org/10.3402/tellusa.v54i1.12121

British Antarctic Survey (2014). *British Antarctic Survey Twin Otter aircraft Meteorological Airborne Science INstrumentation (MASIN) core data for the Aerosol Cloud Coupling and Climate Interactions in the Arctic (ACCACIA) project*. NCAS British Atmospheric Data Centre. https://doi.org/10.5285/0844186db1ba9e20319a2560f8d61651

Burnett, D. (1965). Viscosity and thermal conductivity of gas mixtures. Accuracy of some empirical formulas. *The Journal of Chemical Physics*, *42*(7), 2533–2540. https://doi.org/10.1063/1.1696328

Castellani, G., Lüpkes, C., Hendricks, S., & Gerdes, R. (2014). Variability of Arctic sea-ice topography and its impact on the atmospheric surface drag. *Journal of Geophysical Research: Oceans*, *119*(10), 6743–6762. https://doi.org/10.1002/2013jc009712

Charnock, H. (1955). Wind stress on a water surface. *Quarterly Journal of the Royal Meteorological Society*, *81*(350), 639–640. https://doi.org/10.1002/qj.49708135027

Elvidge, A., Renfrew, I., Weiss, A. I., Brooks, I. M., Lachlan-Cope, T. A., & King, J. C. (2016). Observations of surface momentum exchange over the marginal ice zone and recommendations for its parametrisation. *Atmospheric Chemistry and Physics*, *16*, 1545–1563. https://doi.org/10.5194/acp-16-1545-2016

Fichefet, T., & Maqueda, M. M. (1997). Sensitivity of a global sea ice model to the treatment of ice thermodynamics and dynamics. *Journal of Geophysical Research*, *102*(C6), 12609–12646. https://doi.org/10.1029/97jc00480

Fiedler, E. K., Lachlan-Cope, T. A., Renfrew, I. A., & King, J. C. (2010). Convective heat transfer over thin ice covered coastal polynyas. *Journal of Geophysical Research*, *115*(C10), C10051. https://doi.org/10.1029/2009jc005797

Garbrecht, T., Lüpkes, C., Hartmann, J., & Wolff, M. (2002). Atmospheric drag coefficients over sea ice–validation of a parameterisation concept. *Tellus A: Dynamic Meteorology and Oceanography*, *54*(2), 205–219. https://doi.org/10.3402/tellusa.v54i2.12129

Held, A., Brooks, I. M., Leck, C., & Tjernstrom, M. (2011). On the potential contribution of open lead particle emissions to the central Arctic aerosol concentration. *Atmospheric Chemistry and Physics*, *11*(7), 3093–3105. https://doi.org/10.5194/acp-11-3093-2011

Lock, A., & Edwards, J. (2013). *Unified model documentation paper 24: The parametrization of boundary layer processes. Met Office technical description MetUM version 8.6* (p. 88). Exeter, UK: UK Met Office.

Lüpkes, C., & Birnbaum, G. (2005). Surface drag in the Arctic marginal sea-ice zone: A comparison of different parameterisation concepts. *Boundary-Layer Meteorology*, *117*(2), 179–211. https://doi.org/10.1007/s10546-005-1445-8

Lüpkes, C., & Gryanik, V. M. (2015). A stability-dependent parametrization of transfer coefficients for momentum and heat over polar sea ice to be used in climate models. *Journal of Geophysical Research: Atmospheres*, *120*(2), 552–581. https://doi.org/10.1002/2014jd022418

Lüpkes, C., Gryanik, V. M., Hartmann, J., & Andreas, E. L. (2012). A parametrization, based on sea ice morphology, of the neutral atmospheric drag coefficients for weather prediction and climate models. *Journal of Geophysical Research*, *117*(D13), D13112. https://doi.org/10.1029/2012jd017630

Notz, D. (2012). Challenges in simulating sea ice in Earth System Models. *Wiley Interdisciplinary Reviews: Climate Change*, *3*(6), 509–526. https://doi.org/10.1002/wcc.189

Persson, P. O. G., Fairall, C. W., Andreas, E. L., Guest, P. S., & Perovich, D. K. (2002). Measurements near the Atmospheric Surface Flux Group tower at SHEBA: Near-surface conditions and surface energy budget. *Journal of Geophysical Research*, *107*(C10), 8045. https://doi.org/10.1029/2000jc000705

Petersen, G. N., & Renfrew, I. A. (2009). Aircraft-based observations of air–sea fluxes over Denmark Strait and the Irminger Sea during high wind speed conditions. *Quarterly Journal of the Royal Meteorological Society*, *135*(645), 2030–2045. https://doi.org/10.1002/qj.355

Petty, A. A., Tsamados, M. C., & Kurtz, N. T. (2017). Atmospheric form drag coefficients over Arctic sea ice using remotely sensed ice topography data, spring 2009–2015. *Journal of Geophysical Research: Earth Surface*, *122*, 1472–1490. https://doi.org/10.1002/2017JF004209

Pope, J. O., Bracegirdle, T. J., Renfrew, I. A., & Elvidge, A. D. (2020). The impact of wintertime sea-ice anomalies on high surface heat flux events in the Iceland and Greenland Seas. *Climate Dynamics*, *54*(3), 1937–1952. https://doi.org/10.1007/s00382-019-05095-3

Rae, J. G. L., Hewitt, H. T., Keen, A. B., Ridley, J. K., Edwards, J. M., & Harris, C. M. (2014). A sensitivity study of the sea ice simulation in the global coupled climate model, HadGEM3. *Ocean Modelling*, *74*, 60–76. https://doi.org/10.1016/j.ocemod.2013.12.003

Renfrew, I. A. (2019). *In situ observations of air-sea interaction processes from the Iceland Greenland seas Project (IGP)*. Centre for Environmental Data Analysis. Retrieved from http://catalogue.ceda.ac.uk/uuid/b3e807b8df824a8ca83468ce2e5b54e5

Renfrew, I. A., Barrell, C., Elvidge, A. D., Brooke, J. K., Duscha, C., King, J. C., et al. (2021). An evaluation of surface meteorology and fluxes over the Iceland and Greenland Seas in ERA5 reanalysis: The impact of sea ice distribution. *Quarterly Journal of the Royal Meteorological Society*, *147*, 691–712. https://doi.org/10.1002/qj.3941

Renfrew, I. A., Elvidge, A. D., & Edwards, J. M. (2019). Atmospheric sensitivity to marginal-ice-zone drag: Local and global responses. *Quarterly Journal of the Royal Meteorological Society*, *145*(720), 1165–1179. https://doi.org/10.1002/qj.3486

Renfrew, I. A., Pickart, R. S., Våge, K., Moore, G. W. K., Bracegirdle, T. J., Elvidge, A. D., et al. (2019). The Iceland Greenland Seas project. *Bulletin of the American Meteorological Society*, *100*, 1795–1817. https://doi.org/10.1175/BAMS-D-18-0217.1

Roberts, C. D., Senan, R., Molteni, F., Boussetta, S., Mayer, M., & Keeley, S. P. (2018). Climate model configurations of the ECMWF Integrated Forecasting System (ECMWF-IFS cycle 43r1) for HighResMIP. *Geoscientific Model Development*, *11*(9), 3681–3712. https://doi.org/10.5194/gmd-11-3681-2018

Schröder, D., Vihma, T., Kerber, A., & Brümmer, B. (2003). On the parameterization of turbulent surface fluxes over heterogeneous sea ice surfaces. *Journal of Geophysical Research*, *108*(C6), 3195. https://doi.org/10.1029/2002JC001385

Sigmond, M., Fyfe, J. C., & Swart, N. C. (2018). Ice-free Arctic projections under the Paris Agreement. *Nature Climate Change*, *8*(5), 404–408. https://doi.org/10.1038/s41558-018-0124-y

Stössel, A., Cheon, W. G., & Vihma, T. (2008). Interactive momentum flux forcing over sea ice in a global ocean GCM. *Journal of Geophysical Research*, *113*(C5), C05010. https://doi.org/10.1029/2007JC004173

Strong, C., & Rigor, I. G. (2013). Arctic marginal ice zone trending wider in summer and narrower in winter. *Geophysical Research Letters*, *40*(18), 4864–4868. https://doi.org/10.1002/grl.50928

Stull, R. B. (1988). *An introduction to boundary layer meteorology* (Vol. 13). Springer Science & Business Media.

Tsamados, M., Feltham, D. L., Schroeder, D., Flocco, D., Farrell, S. L., Kurtz, N., et al. (2014). Impact of variable atmospheric and oceanic form drag on simulations of Arctic sea ice. *Journal of Physical Oceanography*, *44*(5), 1329–1353. https://doi.org/10.1175/jpo-d-13-0215.1

Vavrus, S., & Harrison, S. P. (2003). The impact of sea-ice dynamics on the Arctic climate system. *Climate Dynamics*, *20*(7–8), 741–757. https://doi.org/10.1007/s00382-003-0309-5

Yu, X., Rinke, A., Dorn, W., Spreen, G., Lüpkes, C., Sumata, H., & Gryanik, V. M. (2020). Evaluation of Arctic sea ice drift and its dependency on near-surface wind and sea ice conditions in the coupled regional climate model HIRHAM–NAOSIM. *The Cryosphere*, *14*(5), 1727–1746. https://doi.org/10.5194/tc-14-1727-2020